GEOLOGICAL SURVEY OF CANADA
OPEN FILE 8136

Nearbed current and suspended sediment concentration recorded by a seabed lander deployed in the deep water at Sackville Spur, Grand Banks, Newfoundland and Labrador

M. Z. Li, D. J. Schillinger and A. Robertson

2016

Celebrating 175 yrs

Canada

GEOLOGICAL SURVEY OF CANADA
OPEN FILE 8136

Nearbed current and suspended sediment concentration recorded by a seabed lander deployed in the deep water at Sackville Spur, Grand Banks, Newfoundland and Labrador

M. Z. Li[1], D. J. Schillinger[2] and A. Robertson[1]

[1]Geological Survey of Canada (Atlantic)
[2]GaleForce Scientific Consulting Ltd.

2016

Table of Contents

Summary

Powerful near-bed currents exist on the Grand Banks and Labrador slopes down to >1000 m. Field data is lacking in these areas for assessing near-bed current strength and the frequency and magnitude of sediment transport in deep slope waters. The Geologic Survey of Canada-Atlantic (GSCA) deployed a redesigned deep-water seabed lander from August 9 - 21, 2011 in 1200 m water depth on the northern flank of the Sackville Spur, Grand Banks, to collect near-bed currents and sediment transport data. This seabed lander was designed for free-fall type deployment and equipped with a deep-water rated AquaDopp Acoustic Doppler Current Profiler (ADCP) with an analog Optical Backscatter Sensor (OBS) and a camera capable of burst recording both video and still photos of the seabed. The goal of this redesigned lander is to expand our seabed lander technology to make observations of near-bed currents and sediment transport in deep water environments. Assessments of the recorded data indicate that the AquaDopp ADCP ran for the entire deployment and recorded velocity and backscatter profile data as well as suspended sediment concentration at 1.2 m above bottom for ~13 days. Unfortunately, the camera system only recorded seabed images intermittently for the first four days of the deployment due to the premature depletion of the battery power. Analysis of the acoustic backscatter and velocity data recorded by the AquaDopp ADCP shows acoustic interference, likely from the lander frame, contaminating the data of the range from 50 to 60 cm from the transducer. Side-lobe interference from the bottom likely corrupted the bottom three range bins to render the velocity data in the bottom 30 cm unreliable.

The seabed photos show grey mud with possible bioturbation at the lander site.. A cursory evaluation of the seabed images, recorded intermittently from August 9th to 13th, suggests that no apparent sediment transport could be observed during these four days. The preliminary analysis of the ADCP data shows several moderate current events, in which the peak bottom currents reached nearly 30 cm/s. The direction of these peak currents was predominantly to the east. During these moderate current events, the ADCP backscatter intensity (a proxy of suspended sediment concentration) was increased by nearly 50% from the mean background values. A positive correlation between the depth-averaged acoustic backscatter intensity and the depth-averaged current speed was observed. This would suggest that increased current speeds were responsible for the increase of suspended sediment concentration. Profiles of backscatter averaged over the deployment duration show that suspended sediment concentration increases with height above seabed from 0.3 m to 1.3 m above bottom. This suggests that averaged over the deployment duration, the suspended sediments were not bottom intensified and were probably advected from other areas. In the bottom 0.3 m, however, the backscatter amplitude increases rapidly towards the seabed. The profile of the averaged backscatter for current speeds > 0.2 m/s also shows that the backscatter intensity was higher near the seabed and decreased with the increasing height above bottom. This is evidence that local erosion of bottom sediments probably occurred when current speeds exceeded ~0.2 m/s. Nevertheless, the analysis of the data collected is inconclusive whether the increased sediment concentration under increased currents was due to local erosion or being advected to the deployment site from another region. Data from a two day period during the early part of the deployment shows intriguing sinusoidal variations of temperature, current speed and current direction with elevated suspended sediment concentration. Further efforts are warranted to explore the driving processes causing this observed event.

Introduction

Powerful near-bed currents exist on the Grand Banks and Labrador slopes down to >1000 m and are related to the Labrador Current. Knowledge is lacking on how strong the near-bed currents are, and how

they affect frequency and magnitude of seabed scouring and sediment mobility. Existing lander technology was re-designed and modified for deep-water applications. An experimental deep-water lander was successfully deployed and retrieved on Hudson 2011031expedition (Campbell, 2014) to obtain in situ measurements of the nearbed currents and sediment transport in 1200 m depth on the northern flank of Sackville Spur, northern Flemish Pass, in close proximity to the Mizzen significant discovery (Figure 1). The processing and analysis of the lander data collected from this deployment would help our understanding of the intensity of nearbed currents and the magnitude and frequency of resulting sediment mobility as potential constraints to hydrocarbon development in the slope waters of eastern Canada. This Open File report will discuss the innovation effort in developing and testing the deep-water lander technology, the design and deployment operation of the deep-water seabed lander, and the sensors and sampling strategies used for the Sackville Spur deployment. The quality assessment of the data collected and some early findings from the preliminary analysis of the data are then presented.

Deep-water Lander Technology and the Sackville Spur Deployment Operation

The instrumented seabed landers developed at GSCA represent the cutting edge of seabed instrumentation technology for sediment dynamics research and have been deployed in a wide range of coastal, nearshore and shelf environments (Heffler, 1984; Boyd et al., 1988; Li et al., 1997; Li and Amos, 1999; Li and Heffler, 2002; Amos et al., 2003; Puig et al., 2013). Most of these applications of GSCA landers involve sensors rated for depths less than several hundred meters and the technical group has developed a great deal of experience in the deployment and retrieval of seabed landers in these settings. As the geohazards studies in deep waters on the continental slope and in canyons become increasingly important, innovation is needed to incorporate deep-water sensors, re-design seabed lander frames and develop new protocols for the deployment of landers in the deep water environments. GSCA has designed a free-fall deep-water seabed lander for this deployment in 1200 m depth on the northern flank of Sackville Spur, Grand Banks. A Nortek AquaDopp Acoustic Doppler Current Profiler (ADCP) with an Optical Backscatter Sensor (OBS) rated for 2000 m depth had been purchased to measure velocity profile and sediment concentration in waters as deep as 2000 m. A high definition camcorder (BurstCam) illuminated by a Deep Sea Power and LED light suitable for long-duration deep water deployment was developed. Due to the great depth, the traditional approach of using a surface buoy with a mooring rope attached to the lander is not practical. Therefore buoyant floatation devices with acoustic releases and an anchor were developed so that the lander can be deployed in freefall mode and retrieved through acoustically controlled releases.

This re-designed seabed lander for deep water hydrodynamics and sediment transport measurements, shown in Figure 2, consists of a sacrificial train-wheel anchor, and a frame fabricated from aluminum on which oceanographic instruments and mooring accessories are mounted. Atop the frame are four 17" Benthos glass floatation spheres encased in protective plastic "hard-hats" to provide the recovery buoyancy once the deployment was completed. An acoustic release, Benthos 866-A, visible in Figure 2, is located in the centre of the frame and connects the frame to the anchor. Mounted on the frame are both a strobe and iridium-satellite beacon (both mounted vertically amongst the floatation), a 2 MHz Nortek AquaDopp deep water acoustic Doppler current profiler (ADCP, mounted facing down horizontally on image-right just below the floatation), an Optical Backscatter Sensor (OBS, manufactured by Seapoint, mounted on the image-right-front support beam), light (mounted on the image-left-rear support beam) and camera (mounted image-left just below the floatation). Table 1 lists the various sensors, their heights above the bottom, and their purposes and other deployment notes. Table 2 gives the sampling schedules of the key sensors and assessment of the data collected.
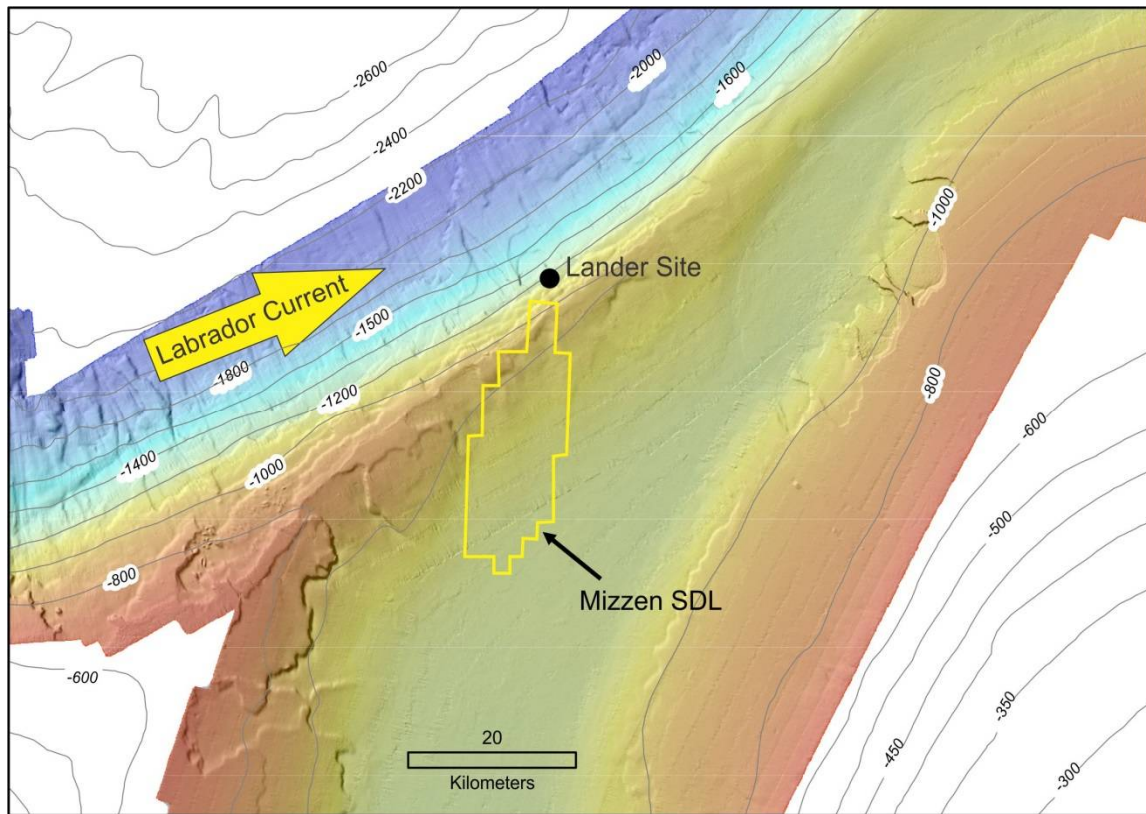
Figure 1 Map showing the location (large black circle) of the deployed deep-water seabed lander on the northern flank of Sackville Spur, northeast of the Grand Banks of Newfoundland. The background shows the multibeam bathymetry courtesy of the Nereida Program. The box marked by the yellow lines is the Mizzen Significant Discovery Lease area.

The lander was designed to freefall to the seabed in deployment. For recovery, the acoustic release is activated via acoustic signal from a transmitter (deck unit) controlled by an operator on the retrieving vessel; upon receipt of the acoustic signal the mechanical release is activated and decouples the frame and floatation from the anchor. Once released the buoyant frame and instruments will ascend to the surface.

For this deployment at Sackville Spur, a second acoustic release was used just above the lander frame (visible in this Figure 2 above the suspended frame). The intent was to lower the lander close to the bed and activate this second acoustic release so that the lander would only free fall for a short distance
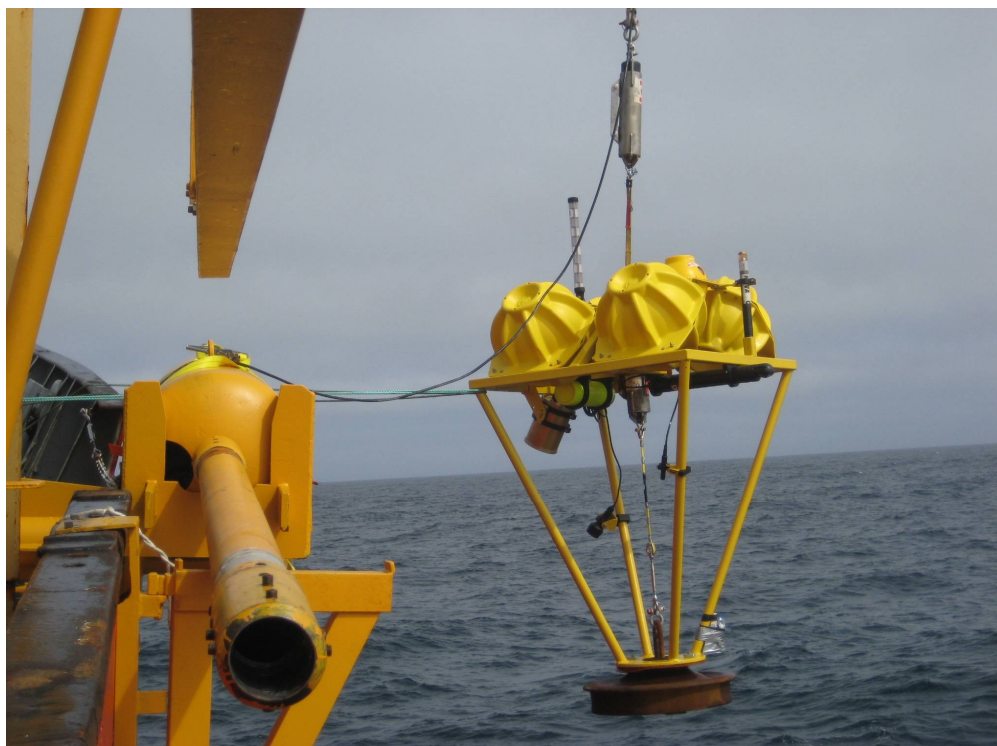
Figure 2 GSCA deep water lander for measurement of currents and sediment transport in the bottom boundary layer.

for improved positioning accuracy. Unfortunately, this operation failed because the release unit was improperly armed at the surface. As a result, the lander broke free from the lowering wire at about 880 m depth, during spooling of the main Pingo winch and freefell to the seabed, resting at a depth of 1199 m at 1430 UTC on August 9th (Lat: 48.431792° N, Lon: 046°.238048 W). The magnetic declination at this location for this date is 18 degrees 18 minutes W.

Recovery was attempted early in the morning on August 21st with some difficulty activating the acoustic release. Finally, a faint confirmation was heard at 1034 UTC and about 20 minutes later just before 1100 UTC the Iridium locator beacon sent a positive email with positioning that the lander was at the surface. The FRC was launched in order to attach a lift strap and the frame was then safely recovered to the foredeck.

Assessments of the recorded data indicate that the AquaDopp ADCP ran for the entire deployment period as programmed. Unfortunately, the camera system did not work entirely as programmed. The seabed was captured on video including the actual freefall touchdown on August 9th at 1430 UTC. The bed appeared to be grey mud and a turbid cloud was raised when the iron ballast train wheel impacted the bed. The camera logged bursts until August13th intermittently and then did not record anymore bursts until back on deck on the 21st. The main battery pack was tested upon recovery and proved to be depleted although it was expected to run for 40 – 60 days. Testing was done in the GSCA laboratories in a cold reefer environment at 4°C in order to replicate the deployment and it was determined that the battery pack used was under capacity for a two week deployment, including a lengthy pre-deployment test.

Instrument	Height above bottom (m)	Purposes and deployment notes
AquaDopp	1.62	Current velocity profiles; also records co-located heading/attitude/pressure
OBS	1.23	Attached via cable to analog port of AquaDopp for suspended sediment concentration at a fixed height
Camera	1.45	Pointed at 70° downward; Provides information of seabed type, seabed responses and sediment transport modes;
Matrix LED lights	0.92	
Sediment trap	0.4	Grain size of resuspended sediments and sedimentation layers for the duration of deployment;

Table 1: Vertical position of instruments (height above bottom), purposes and deployment notes

Instrument	Sampling schedule and data recorded
AquaDopp/OBS	Records velocity profiles at 1 Hz continuously; Each profile consists of 17 10 cm cells with a 10 cm blanking zone immediately below the ADCP; Recorded data for 12 days over the entire deployment duration.
Camera/Lights	1 still image followed by 5 seconds of video on the hour and 15 minutes past the hour; Only 2 days of data recorded, not analysed.
Sediment trap	Continuous; Samples spilled during recovery.

Table 2: Sampling schedules and assessment of data recorded.

Quality Control

The AquaDopp ADCP velocity data sampled at 100% measurement load and recorded at 1 Hz ensemble averages has an uncertainty of 30.9 cm/s. Averaging ensembles together reduces this uncertainty by the square root of N, where N is the number of ensembles in the average. Unless otherwise stated, the data presented in this report are averages of 10 minutes of non-overlapping data. Matlab files with 1 minute averaged data have been obtained for evaluation of the presence of internal waves. For the 10 minute average interval, 600 ensembles were averaged, reducing the uncertainty in horizontal velocity to 1.26 cm/s.

Acoustic Doppler current profilers capable of resolving velocities in three dimensions consist of at least three transducers configured in three orthogonal orientations. The transducer geometry, fixed through manufacturing, allows the transformation of the measured along-beam velocities to an XYZ frame of reference relative to the instrument; the instrument attitude and orientation is required to rotate this XYZ frame of reference to what's called an East/North/Up frame of reference (or ENU). All values presented in this report have been rotated to be relative to true north. With this in mind, the first measure of data quality is an analysis of heading and orientation. Time series of 10 minute ensemble averages of pressure (top), heading (second from top), pitch (third from top), roll (second from bottom) and

temperature (bottom) are shown in Figure 3. The on-board compass has been calibrated to account for magnetic offsets due to the frame and the battery pack and thus records values in compass degrees relative to magnetic north.

Over the first few hours of the deployment, the pitch settled from -5.3 to -5.1degrees and the roll settled from -1 to -0.5 degrees. Pitch is the angle measured from the vertical of the axis running the length of the instrument, while roll is measured as the angle of the axis running perpendicular to the instrument body. A negative pitch indicates that forward beam (beam 1) was angled toward the ocean bottom; a pitch of -5 degrees corresponds to an acoustic path length of beam 1 fifteen centimeters shorter than the two outboard facing transducers.

The heading stayed stable over this settling period, and then oscillated from 172 to 172.5 degree over the course of the deployment. Also evident from Figure 3 is an event in which the temperature oscillated between 4 and 3.5 degrees three time over two days (Year-day 223 to 225); the temperature oscillation does not seem to be related to the phase of the tide (compare to the time series of pressure).

A second measure of data quality for acoustic profilers is the acoustic backscatter signal from each of the transducers. Acoustic backscatter converted from engineering units (using 0.5 dB/count; a more complete analysis would use transducer specific numbers which range from 0.4 to 0.47 dB/count, but the backscatter signal has not been calibrated and in a single frequency unit there is significant ambiguity caused by the sediment size distribution) and adjusted to account for spherical spreading and absorption loss along the transit path for beams 1 (top) through 3 (bottom) are shown in Figure 4. In each subplot, time is presented along the x-axis and range from the transducer along the y-axis; the colour represents the relative strength of the backscatter signal with large amplitude backscatter events shown in red and low amplitude signals in blue.

Most concerning in this plot is the discontinuity in backscatter values in beam 3, shown by the light blue streak occurring at a range of 0.6 m. Backscatter levels at this range for this beam are elevated with respect to the values of adjacent range bins. The water-sediment interface has a large reflection coefficient and can be clearly seen as the large stationary reflector in each of the three beams. The difference in the apparent height above bottom (HAB) is consistent with the 5.5 degree pitch of the instrument. A higher than background signal is present immediately above the water-sediment interface in each of the beams, although this feature is masked by the chosen colour scale. Figure 5 shows only four bins near the interface, with the colour bar reflecting a smaller range in acoustic backscatter and backscatter amplitude being corrected for range and attenuation losses. Figure 5 shows that the water-sediment interface is at a range of 1.5 m for beams 1 and 2 and 1.6 m for beam 3. Another, perhaps more clearly demonstrated, version of this data is presented as a mean profile plot in Figure 7.

Colour plots of the east/west (top), north/south (middle) and vertical velocity as a function of time (x-axis) and range (y-axis) are shown in Figure 6. Velocities to the east (top), north (middle) and up (bottom) are indicated by shades of red while negative velocities (i.e. to the west, south and down) are shown by shades of blue. The effects of the acoustic interference from beam 3 are evident in all three components of velocity at 0.5-0.6 m range. Also evident is that the velocity measurements in near bottom bins are corrupt. The velocity field changed in all three components during the time period where the abrupt changes in temperature occurred. An analysis of the relationship on current direction and water temperature follows in the data analysis section.

The effects of the acoustic interference are, perhaps, better demonstrated in a profile plot. The average horizontal and vertical current speeds (left) and raw backscatter (right) over the duration of the deployment are calculated for each depth in Figure 7. The location of the bottom as defined by the height of the AquaDopp ADCP relative to the train wheel (1.62 m) is shown in both plots as the solid black line, while the location of the acoustic bottom for two beams (1.5 m) is shown as the dashed black line. Data from all depth bins are shown by symbols. Both the horizontal and vertical speed profiles show an increase in speeds with depth for ranges greater than 1.2 m; this behavior is likely due to sidelobe interference from the water-sediment interface. The data point for horizontal velocity at 1.4 m range is not shown (it is off scale at over 1.94 m/s). Data points which have not been rejected for use in the log-profile estimates of bottom drag coefficient based on the analysis of backscatter are connected with solid lines; profile data for backscatter amplitude are connected by lines through all data points to highlight the different distances to the backscatter maximum, and the different thicknesses of the elevated backscatter levels near-bottom.

Data Analysis

There are several main features that need to be discussed with respect to this data set.

1) seabed type and magnitude and direction of measured bottom currents
2) temperature/direction related event
3) depth averaged acoustic backscatter is well correlated with depth averaged velocity
4) backscatter intensities: bottom intensification or advection
5) bottom drag estimates have been calculated using log-profiles of the horizontal speed; however, profile shapes are less than ideal

Seabed type and magnitude and direction of measured bottom currents

The still seabed photos at selected times (Figure 8) show that the bottom sediment at the deployment site in 1200 m depth was grey mud with possible bioturbation. The initial check of the seabed photos recorded intermittently from 1500 August 9 to 0500 August 13 indicates that no apparent sediment transport could be observed during these four days. However, small changes did occur periodically (Figure 8). It is unclear whether these changes were caused by near-bed currents or biological activities.

The time series of the profiles of the U and V components in Figure 6 and the time series data of the depth-averaged current speed and direction in Figure 11 demonstrate that there were several moderate current events in which the peak bottom currents reached nearly 30 cm/s. The direction of these peak currents was mostly to the east and likely reflects the direction of the Labrador Currents at this location. During the period of temperature oscillations (year-day 223 to 225), however, the peak currents were dominantly to the southeast.

Sediment concentration

The acoustic backscatter data is well correlated between all three beams. Correlation values were calculated between beam 1 and 2, 1 and 3 and 2 and 3 for both depth averaged values and for the third bin from the transducer. The correlation coefficient R values were 0.99 in all cases.

Acoustic backscatter data can be used as qualitative estimates of sediment concentration in the water-column. Assuming a size distribution of scatterers independent of depth, backscatter data can be used to

present both a vertical distribution and a time series distribution of scatterers (suspended sediment).

Profiles of backscatter averaged over the entire duration of deployment in Figure 7 show that backscatter amplitude increases from ~70 to ~100 counts for distance range from 1.2 m to 0.2 m range. This relationship would suggest that for the long-term conditions averaged over the deployment duration, the suspended sediments in the water column were not bottom intensified and were probably advected to the deployment site from another area. For the 1.2 to ~1.5 m distance range, however, the backscatter amplitude shows significant increase from 70 to 200 counts. This suggests rapid increase of suspended sediment concentration near the water-sediment interface albeit the possibility that the backscatter data of the near-bottom bins could be partially affected by the high reflection of the bottom.

Figure 9 shows three profile plots of speed (left) and backscatter (right) averaged for the velocity ranges indicated in the legend. It is evident from this plot that backscatter levels increase with increasing speed. The profiles of the averaged backscatter for speed <0.1 m/s and for speed between 0.1 – 0.2 m/s seem to show that backscatter intensity increases slightly with increasing height above bottom, suggesting that suspended sediments under these conditions were advected to the deployment site from other areas. However, the profile for speed >0.2 m/s shows higher backscatterance (38 – 39 dB) near the bottom (0.8 – 1.2 m range) and the backscatterance decreasing to ~36 dB from 0.8 m to 0.2 m range. This would suggest that when near-bed current speeds are >0.2 m/s, there is a well-mixed bottom layer of higher suspended sediment concentration (SSC) and the SSC then decreases with increasing heights above bottom. This would suggest that local resuspension likely occurs when near-bed currents reach 0.2 m/s or higher. Correlating depth averaged speed, to depth averaged backscatter of all data, yields a surprisingly low R (R=0.46). Data analysis in the next section show a time period where high backscatter values occur independent of speed, presumably being advected in from another region. When this time period is excluded the correlations improve (R= 0.82).

OBS measurements

Optical backscatter sensors are known to suffer from data spikes. To remove the effects of anomalous data spikes from averaged data, a threshold based exclusion algorithm was used to process the OBS data. Figure 10 shows the raw data (top), averaged data (middle), and averaged despiked data (bottom) from the optical backscatter sensor.

Optical backscatter can be related to the acoustic backscatter signal of the ADCP. Comparisons of the depth averaged acoustic backscatter to the averaged despiked optical backscatter measured by the OBS yields a correlation coefficient R=0.64 (lower left, Figure 12).

Temperature Event

Figure 11 shows several time series plots which relate the period where temperature oscillated between 3.5 and 4 degrees (grey segment) mentioned in the quality control section. This period also corresponded to a period of elevated backscatter, and a sinusoidal change in current direction with a period of about a day, lasting for about 2 days.

Figure 11 aims to show that the temperature is not related to the phase of the tide, shown by plotting alongside the pressure signal (top panel). Depth averaged speed and depth averaged backscatter during this time period of temperature oscillation were largely positively correlated with occasional divergences (middle panel), while depth averaged current direction and temperature were several hours out of phase,

but were clearly linked (third panel from top). Scatter plots of depth averaged speed versus depth averaged backscatter (bottom left panel) show a tight linear relationship for times outside this temperature event (blue dots). Time when the temperature was varying (red dots) shows weak relation, while there was a settling period of nearly 1 day after the temperature event where backscatter levels apparently settled out (green dots). There is no relationship between elevated backscatter levels and temperature (bottom right panel).

Figure 12 probes the relationship between optical backscatter and this event, and by doing so, compares optical to acoustical measures of backscatter (or suspended sediment concentration). The top panel of this figure is a repeat of the temperature and direction plot showing the relationship between the oscillating temperature signal and the depth averaged current direction. The second panel shows time series of acoustic backscatter and optical backscatter. The OBS and ADCP backscatter data track well, although there are periods where the OBS measures an increase in backscatter levels that the AquaDopp does not. This leads to the low correlation value of R=0.64 between optical and acoustical measures of backscatter, shown by a weakly linear relation (bottom left panel). Depth averaged speed and optical backscatter are similarly weakly related (bottom right panel), although the relationship would improve if data points during the temperature event were excluded.

Estimates of bottom shear stress and drag coefficient

The bottom shear stress was estimated by first fitting a first order polynomial to log profile plots. Profiles of horizontal speed were generated by binning the speeds based on the depth mean speed over the range of 6.5 cm/s to 26 cm/s in 1 cm/s intervals. These profiles are shown in Figure 13, where U is the speed at 1.1m height above bottom. Bottom shear stress τ relates to bottom current speed U through the quadratic stress law:

$$\tau = \rho u_*^2 = \rho C_D U^2$$

where ρ is water density, C_D is bottom drag coefficient, u_* is shear velocity which is the shear stress expressed in velocity unit. u_* is estimated as the slope of the linear regression fitted line of ln (z) and U with z representing the height above the seabed, and the bottom roughness length z_o is determined by the intercept. The fitting process was repeated using all data points and various selections of data points in each profile. Solid squares in Figure 13 show the data points which were used for each profile, while squares and lines show all data points. Red indicates that the profile was excluded from the next step. Table 3 shows U, u_*, z_0, and R (regression coefficient) as determined from log-profile fitting for each profile.

Figure 14 shows the relationship between U^2 and u_*^2. Again, red indicates that the value of u_* determined from the log profile was excluded. The best fit, passing through the origin is shown as the solid line. The bottom drag coefficient C_D, determined from the slope of the best fit, is 3.5 x 10^{-3}.

U	zo	R	U*
0.1039	0.2367	0.9119	0.0251
0.1088	0.1496	0.9198	0.204
0.1213	0.1044	0.9767	0.0181
0.1228	0.0199	0.7951	0.0104
0.1373	0.0093	0.9155	0.0094
0.1495	0.0129	0.8726	0.0113
0.1544	0.0093	0.9469	0.0114
0.1666	0.0049	0.9099	0.0107
0.1724	0.0040	0.9431	0.011
0.1836	0.0044	0.9467	0.012
0.1880	0.0050	0.9589	0.0132
0.1996	0.0018	0.9849	0.0117
0.2091	0.0011	0.9908	0.0114
0.2200	0.0024	0.9891	0.0136
0.2331	0.0005	0.9985	0.0112
0.2385	0.0012	0.9901	0.0132
0.2507	0.0014	0.9864	0.0143
0.2607	0.0023	0.9565	0.0162
0.2725	0.0013	0.9770	0.0153
0.2851	0.0012	0.9848	0.0159

Table 3: Table listing the values of U, the speed at 1.1 m HAB, Z0, R, and U* as determined from the log profile regression.

Discussion

The question arises as to why the log profiles do not clearly show the interface to the bottom boundary layer (i.e. a clearly linear region in the log profile plot, above which the velocities behave differently). We attempted to improve the profile plots by eliminating times when the flow was from certain directions. This did not produce improved analysis. Figure 15 shows a scatter plot of the horizontal velocity (dots) and the orientation of the AquaDopp (solid line). It is clear that the majority of the flow is passing over the frame, shedding eddies from the train-wheel, the aluminum support rods, or the floatation. While it is not apparent from this figure that all beams would be affected by turbulence from the frame for all directions, it is clear that beam 2, the port side outboard beam on the AquaDopp (Figure 2), would be clearly in the downstream field for the majority of the measurements. The time series of profiles of the current components in Figure 6 and the profiles of speed averaged over the duration of deployment, presented in Figure 7, indicate that side-lobe interference from the bottom likely corrupted the bottom three range bins, at least affecting the velocity data in the bottom 30 cm. The cause(s) of this interference needs to be investigated and the design should be improved so that this issue can be eliminated in the future,

The deep-water lander deployed on the slope off Sackville Spur recorded several moderate current events in which the peak bottom currents reached nearly 30 cm/s (Figure 11). The direction of these peak currents was generally to the east except during the period of temperature oscillations. During these

moderate current events, the ADCP backscatter intensity (a proxy of suspended sediment concentration) was increased by nearly 50% from the mean background values. Both the time series (second panel of Figure 11) and the scatter plot (bottom left panel of Figure 11) demonstrate good positive correlation between the depth-averaged acoustic backscatter intensity and the depth-averaged current speed, which suggests that increased current speeds were responsible for the increased suspended sediment concentration. Profiles of backscatter averaged over entire duration of deployment in Figure 7 show that suspended sediment concentration increases with height above seabed from 0.3 m to 1.3 m above bottom. This relationship would suggest that for the conditions averaged over the deployment duration, the suspended sediments in the water column were not bottom intensified and were probably advected to the deployment site from another area. Although, there is the possibility that the backscatterance of the near-bottom bins was partially affected by the high reflection coefficient of the seabed; the backscatter amplitude in the bottom 0.3 m shows rapid increase towards the seabed which would mean that suspended sediments were from local seabed erosion. When backscatter was averaged for different velocity ranges (Figure 9), the profiles of the averaged backscatter for current speeds <0.2 m/s show that the backscatter intensity tends to increase slightly with increasing height above bottom. The profile of the averaged backscatter for current speeds > 0.2 m/s, however, shows that the backscatter intensity was higher near the seabed and decreased with the increasing height above bottom. The analysis of the data collected is thus inconclusive whether the increased sediment concentration under increased currents was due to local erosion or being advected to the deployment site from another region.

The two day periods with significant temperature oscillations (Year-day 223 to 225; Figure 11) show intriguing variations of temperature, current speed and direction, and suspended sediment concentration. In comparison with the background temperature of ~3.8° and current direction of ~90°, this period showed sinusoidal variation of temperature between 3.6 to 4.0°and of current direction between 30° to 170°. The sinusoidal variation had a period of about one day and lasted for about two days. The comparison between the pressure and temperature (top panel of Figure 11) indicates that the temperature changes were not related to the phase of the tide. Current speed, direction and temperature were roughly in phase with slight offsets during this period. During the phase of increasing current speed, the current direction changed from 30° to 170° while the temperature increased from 3.6 to 4.0°. During the phase of decreasing current speed, the values of current direction and temperature would reverse. While the peak current speeds during this period were similar or slightly lower than that for times outside the temperature event, the backscatter intensity was elevated and reached the highest values of ~45 dB for the entire deployment duration. The driving processes causing the observed event of oscillating temperature and current direction with elevated sediment concentration are worthy of further exploration.

Acknowledgements

References

Amos, C. L., M. Z. Li, F. L. Chiocci, G. B. La Monica, S. Cappucci, E. H. King, and F. Corbani, 2003. Origin of shore-normal channels from the shoreface of Sable Island, Canada, J. Geophys. Res., 108(C3), 3094, doi:10.1029/2001JC001259.

Boyd, R., D.L. Forbes and D.E. Heffler, 1988. Time sequence observations of wave-formed sand ripples on an ocean shoreface. Sedimentology, 35, 449-464.

Campbell, D.C., 2014. CCGS Hudson expedition 2011-031, Flemish Pass and Salar Basin, August 6-22, 2011; Geological Survey of Canada, Open File 7145, 102 p. doi:10.4095/293699

Heffler, D.E., 1984. RALPH - An instrument to monitor seabed sediments. Current Res. Part B, Geol. Surv. Can. Pap. 84-lb, 47-52.

Li, M.Z. and Amos, C.L., 1999. Field observations of bedforms and sediment transport thresholds of fine sand under combined waves and current. Marine Geology, 158, 147-160.

Li, M.Z. and Heffler, D.E., 2002. Continental Shelf Sediment Transport Studies in Canada: Basic Theories and Recent Technology Advances. Environmental Marine Geoscience 3, Geoscience Canada, 29, 35-48.

Li, M.Z., Amos, C.L. and Heffler, D.E., 1997. Boundary layer dynamics and sediment transport under storm and non-storm conditions on the Scotian Shelf. Marine Geology, 141, 157-181.

Puig, P., Greenan, B.J.W., Li, M.Z., Prescott, R.H. and Piper, D.J.W., 2013. Sediment transport processes at the head of Halibut Canyon, Eastern Canada margin. Marine Geology, 341, 14-18.
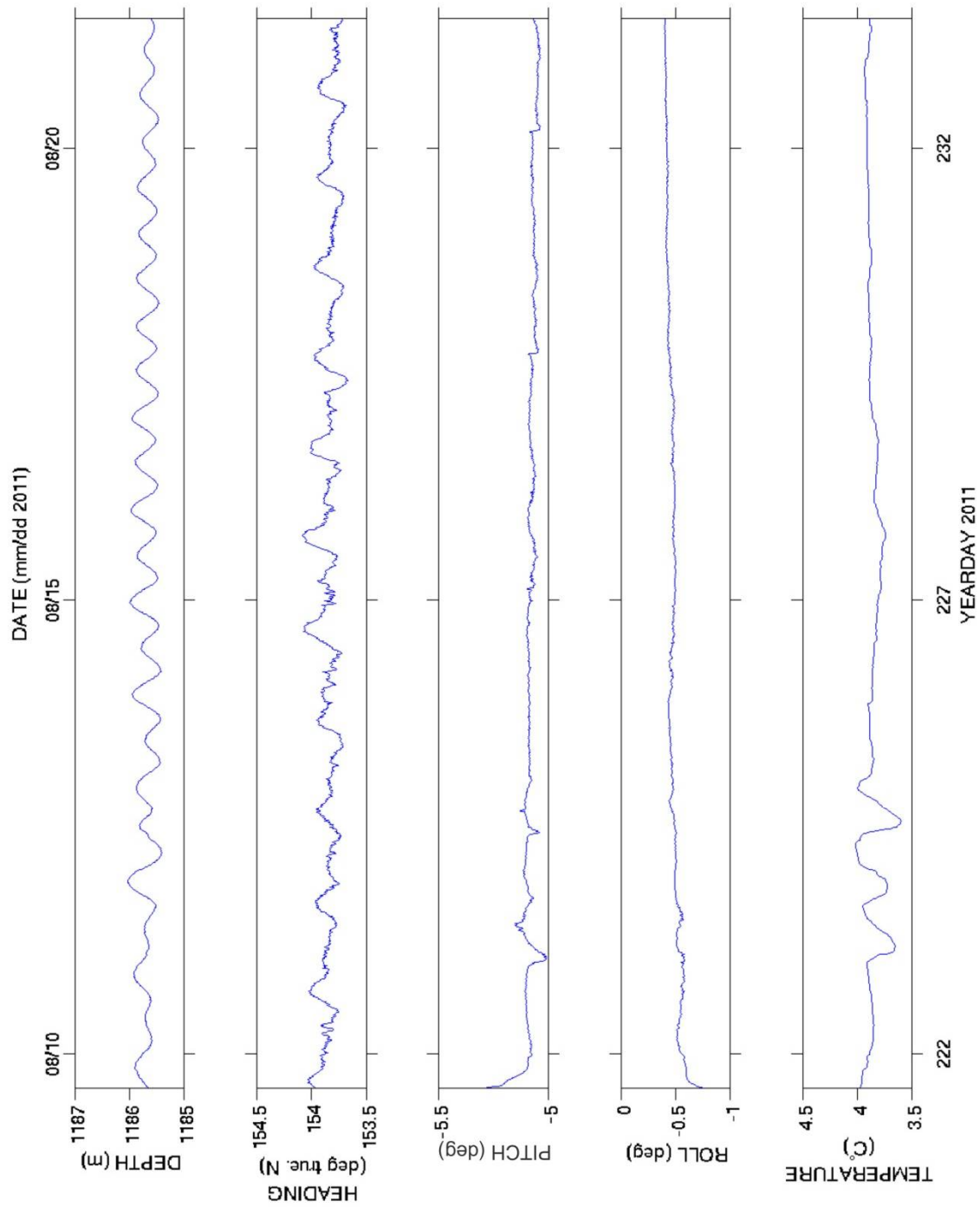
Figure 3 Time series of depth (top), heading (second), pitch (middle), roll (second from bottom) and temperature (bottom), as measured by the AquaDopp. Values are 10 minute ensemble averages.
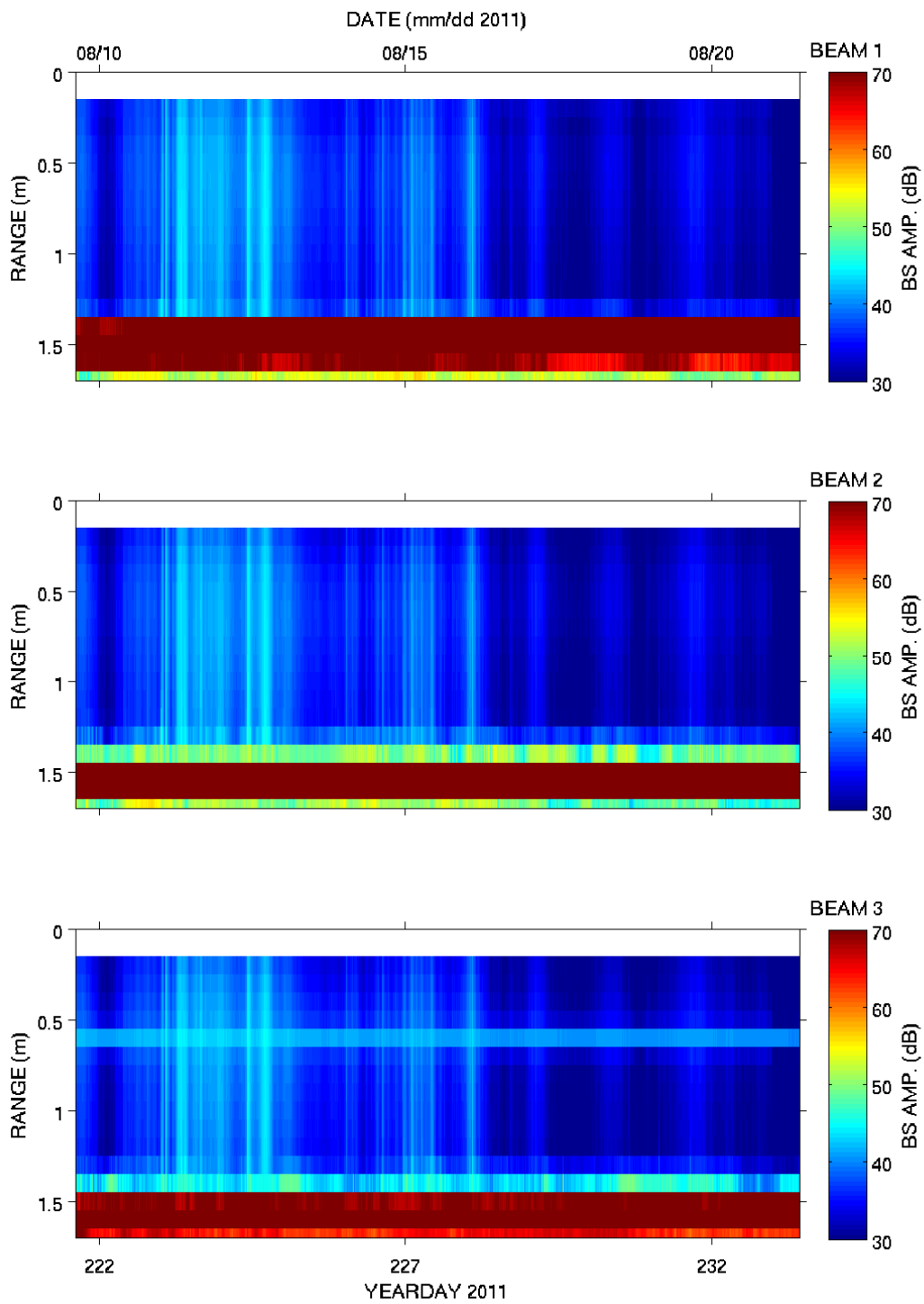
14

Figure 4 Backscatter amplitudes (arb. dB), corrected for range and attenuation losses, for beams 1 (top) to 3 (bottom) of the AquaDopp profiler.
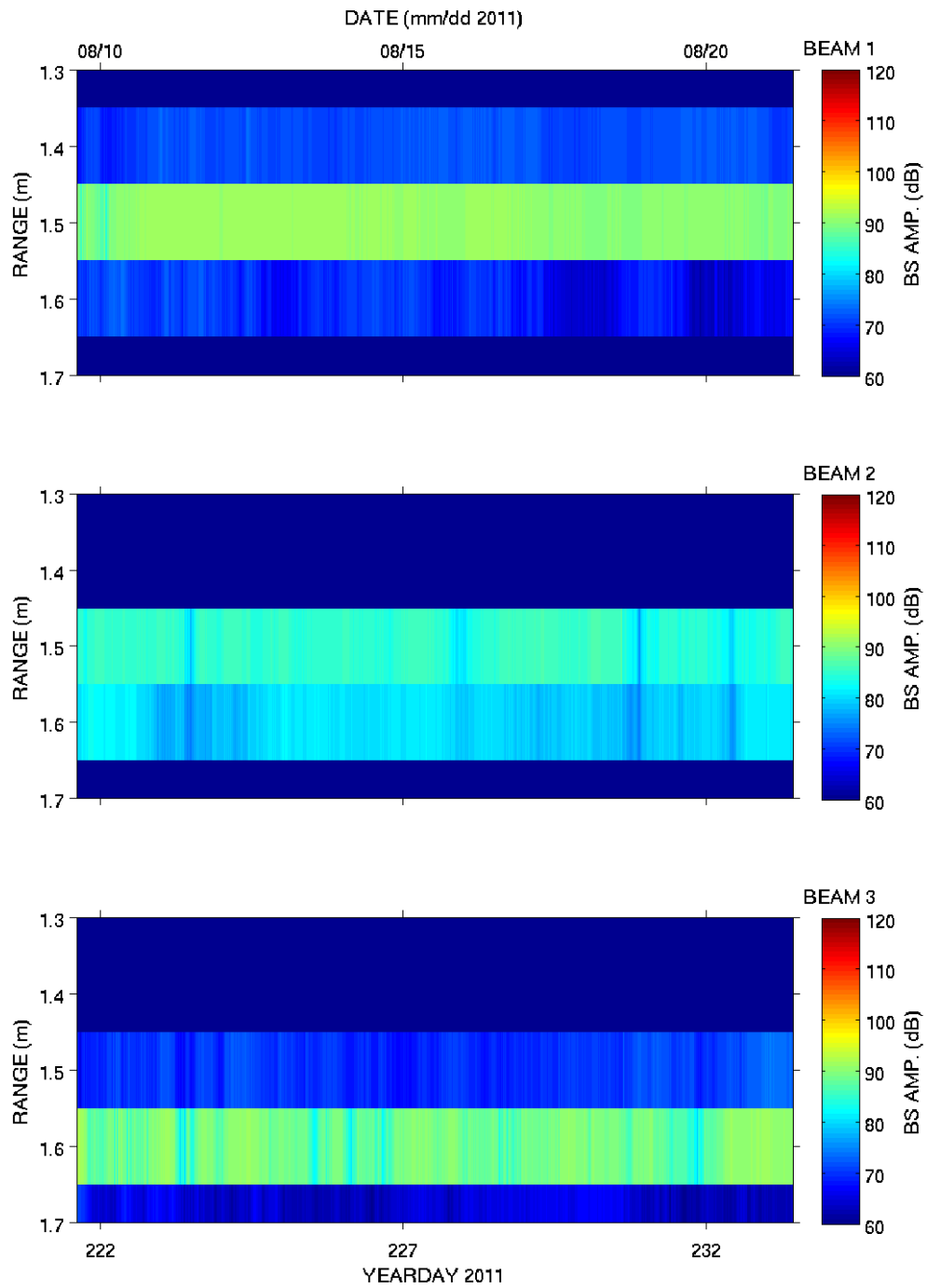
Figure 5 Backscatter amplitudes (arb. dB), corrected for range and attenuation losses, for beams 1 (top) to 3 (bottom) of the AquaDopp profiler for the 4 bins nearest the largest backscatter signal (the ocean-sediment interface).
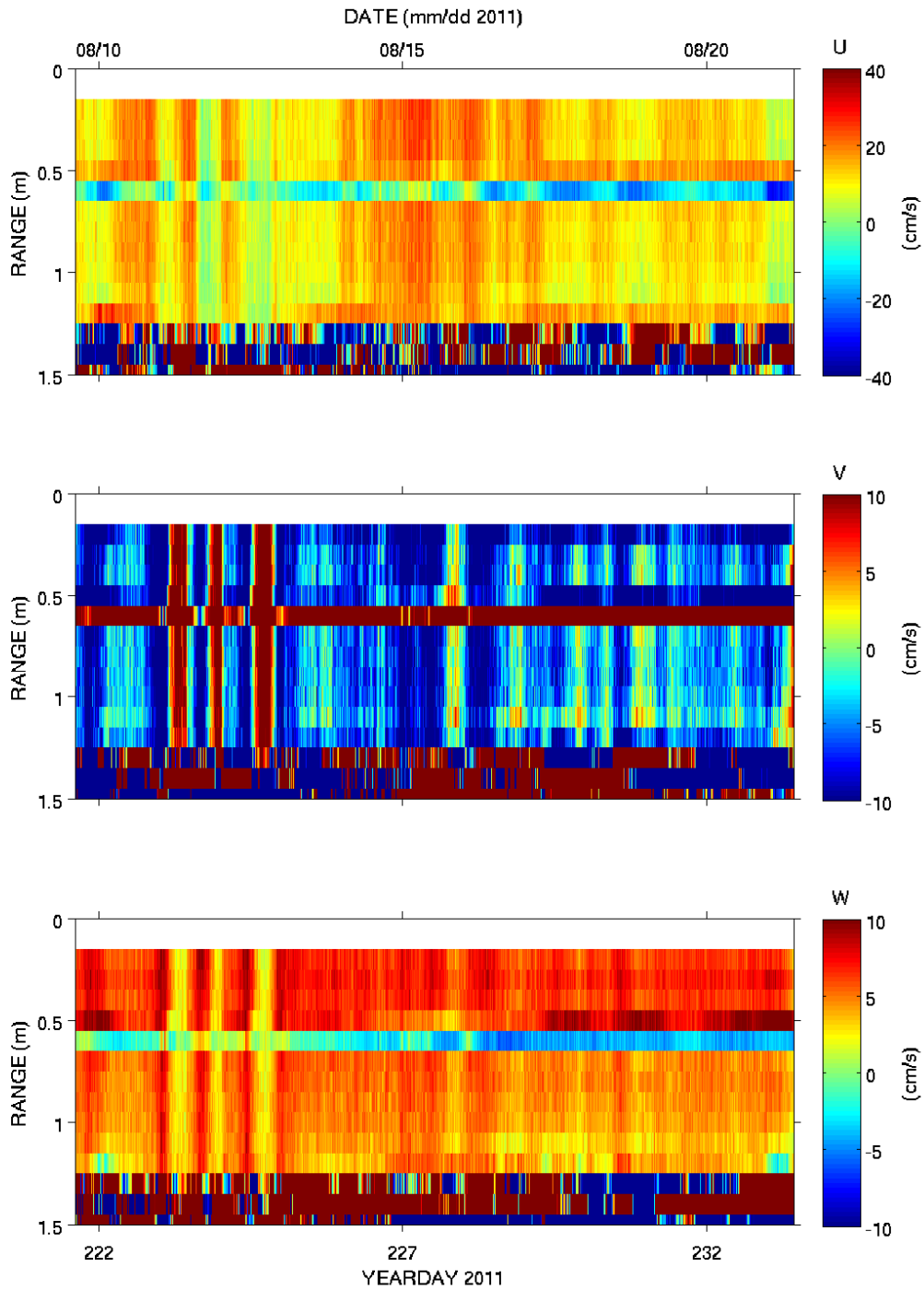
Figure 6 U (east/west, top panel), V (north/south, middle panel), W (up/down, bottom panel) velocity measured by the AquaDopp profiler. Figure shows 10 minute average ensembles. East, north and up are represented by positive (red) velocities.
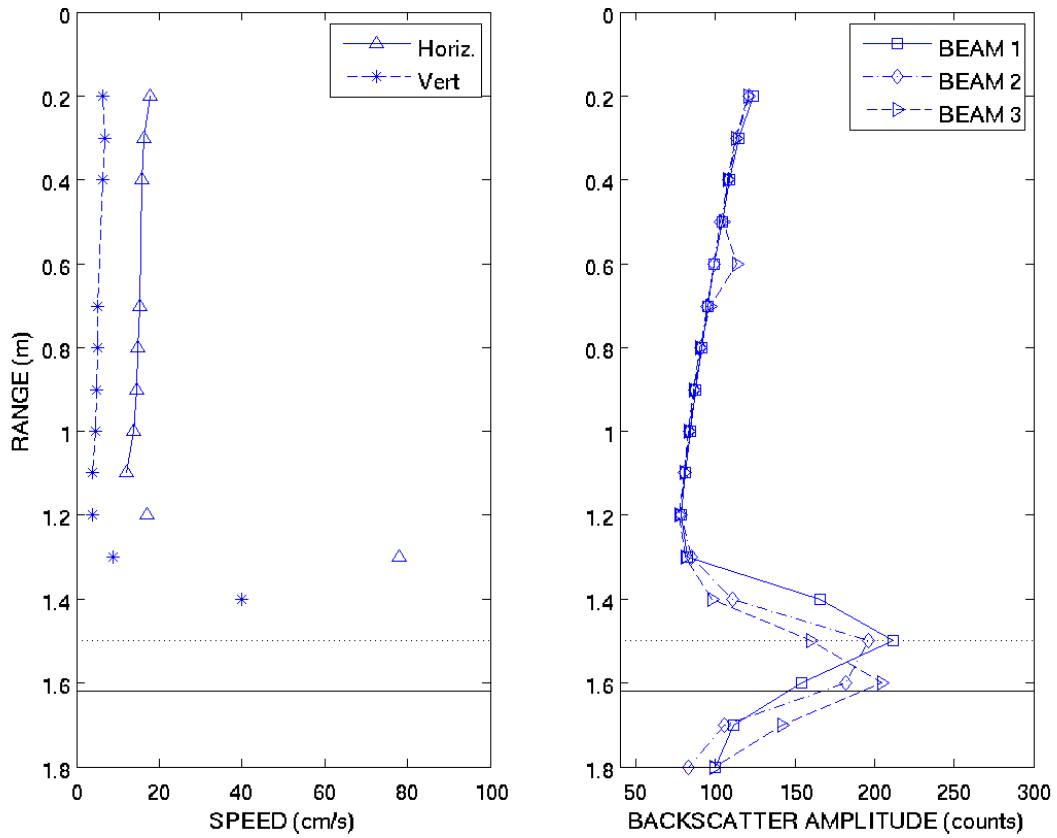
Figure 7 Profile of speed (left) and raw backscatter (right) averaged over entire duration of deployment. Horizontal (triangle) and vertical (asterix) speeds are plotted in the left panel; data points corrupted by side lobe interference are shown as symbols only. Backscatter for beams as indicated by the legend in plot on the right.

Figure 8 Seabed photos taken at (top) 0500 August 10 and (bottom) 1430 August 12, 2011.
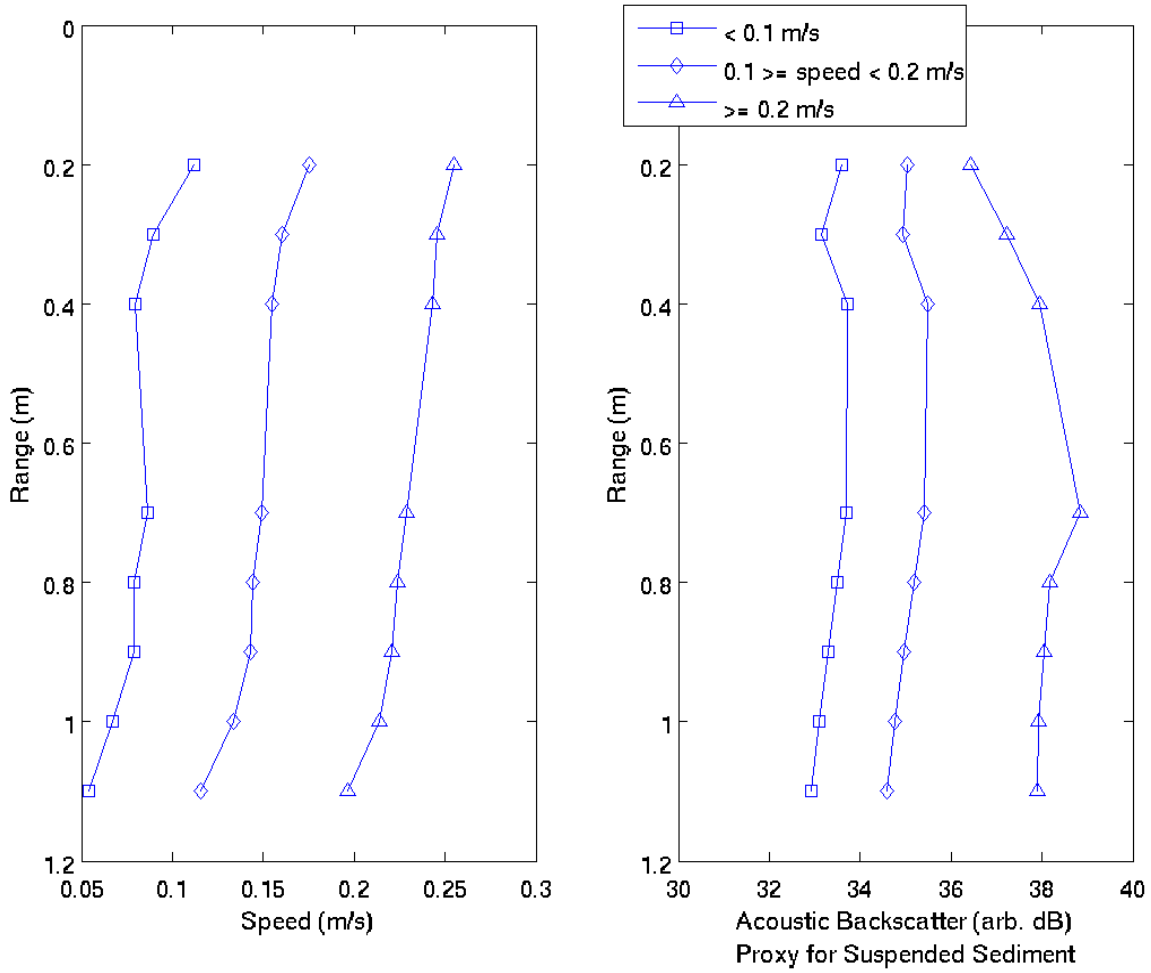
Figure 9 Profiles of mean speed (left) and mean acoustic backscatter (right) for the velocity ranges indicated in the legend. The acoustic backscatter signal is meant to represent the suspended sediment concentration. Profiles are plotted as range from the AquaDopp.
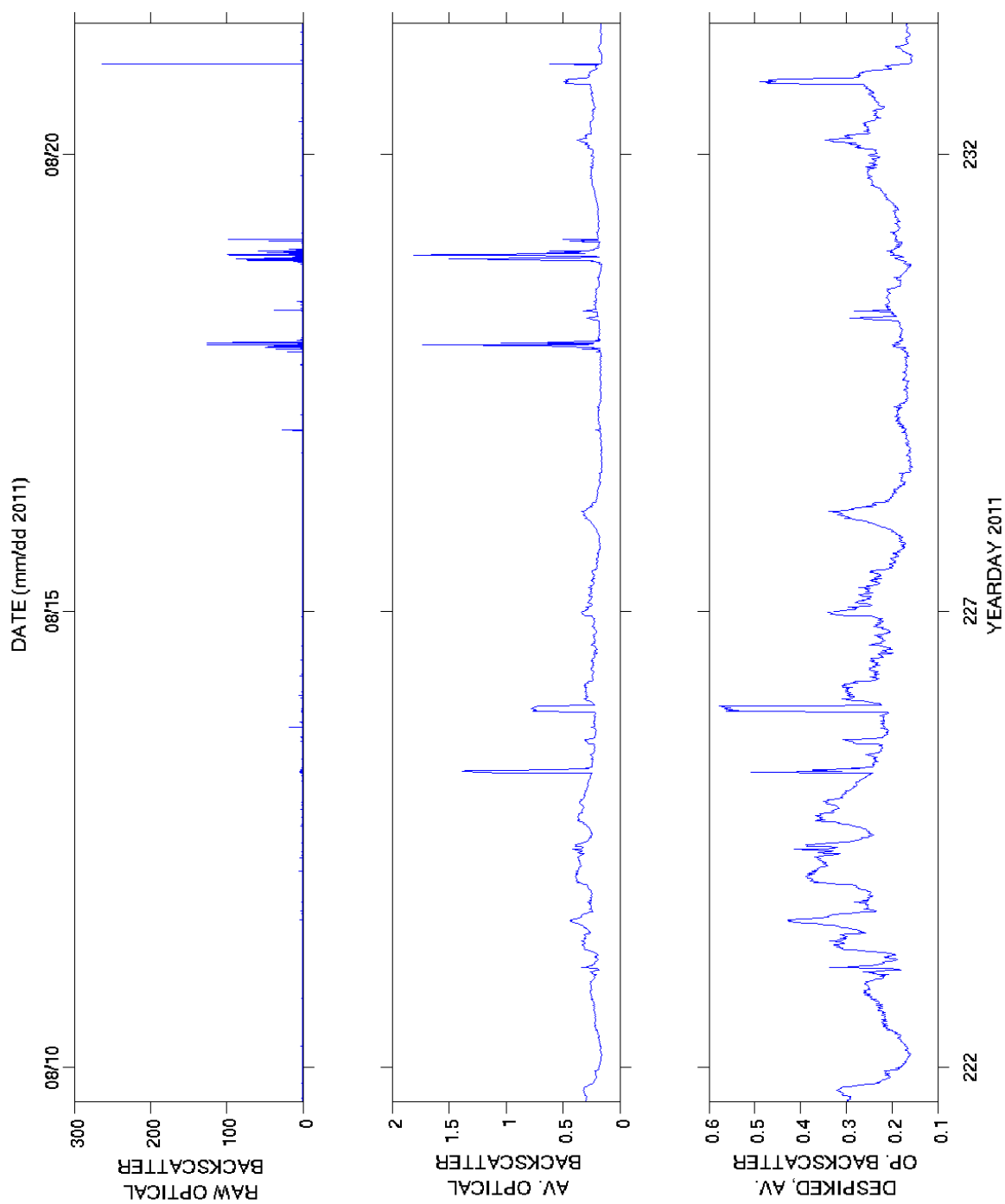
Figure 10 Raw (top), averaged (middle), despiked and averaged (bottom) OBS data. All plots are in FTU. FTU stands for Formazine turbidity unit, an uncalibrated measure of suspended sediment concentration.

21
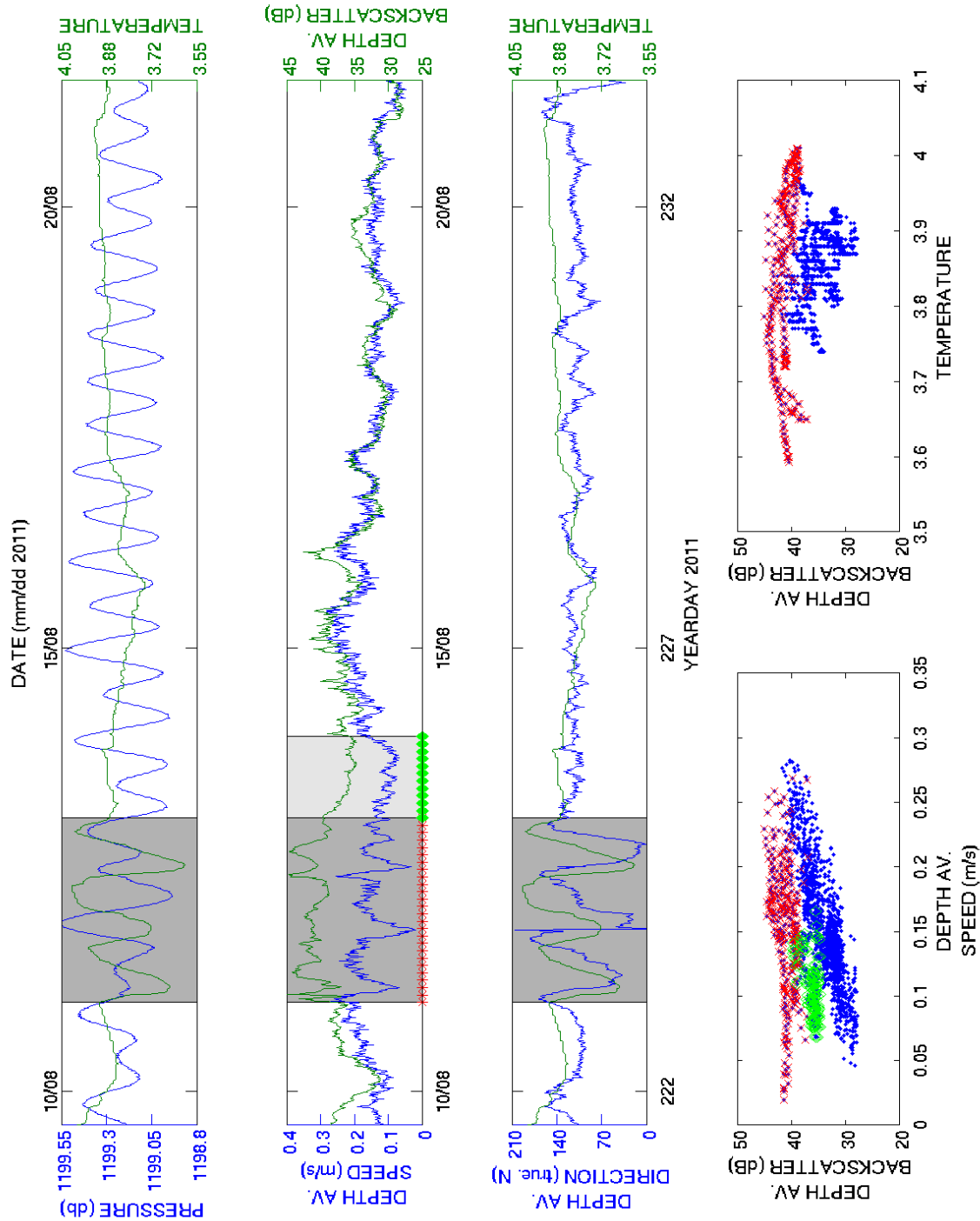
Figure 11 Time series of pressure and temperature (top plot), depth averaged speed and acoustic backscatter (second panel), and depth averaged current direction (true north) and temperature (third panel) with an event shown in grey. Red and green points delineate two time regions in the time series plots, and correspond to points in the lower two scatter plots. The bottom panel shows scatter plots of depth averaged backscatter versus speed (left) and depth averaged backscatter versus temperature (right).
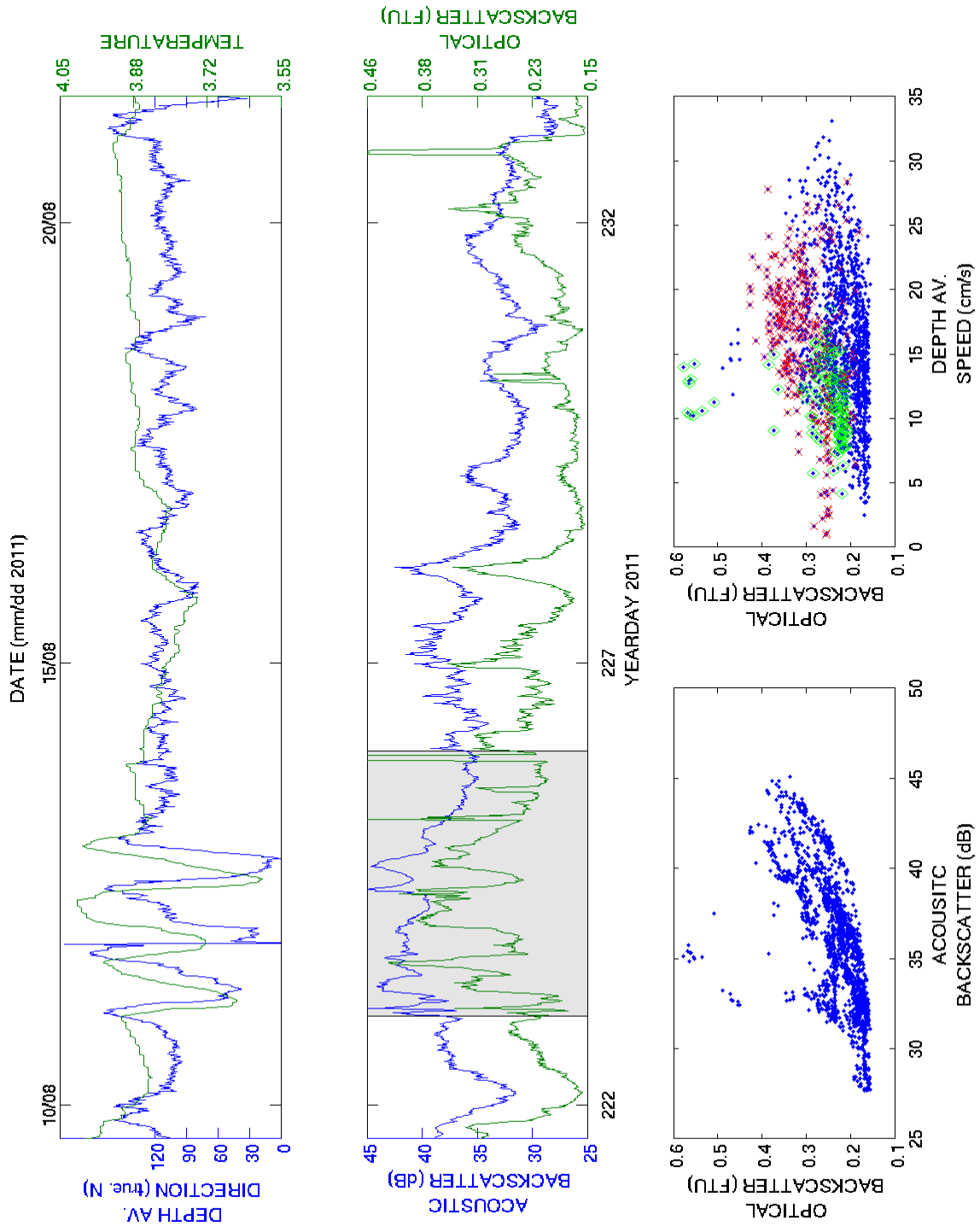
Figure 12 Depth averaged current direction and temperature (top), depth averaged acoustic backscatter and optical backscatter (second) time series plots. The event from Figure 11 is shown in grey. Scatter plots of backscatter versus optical backscatter (left) and optical backscatter versus depth averaged speed (right) are shown in the bottom panels. Red × and green diamonds indicate times as per Figure 11.
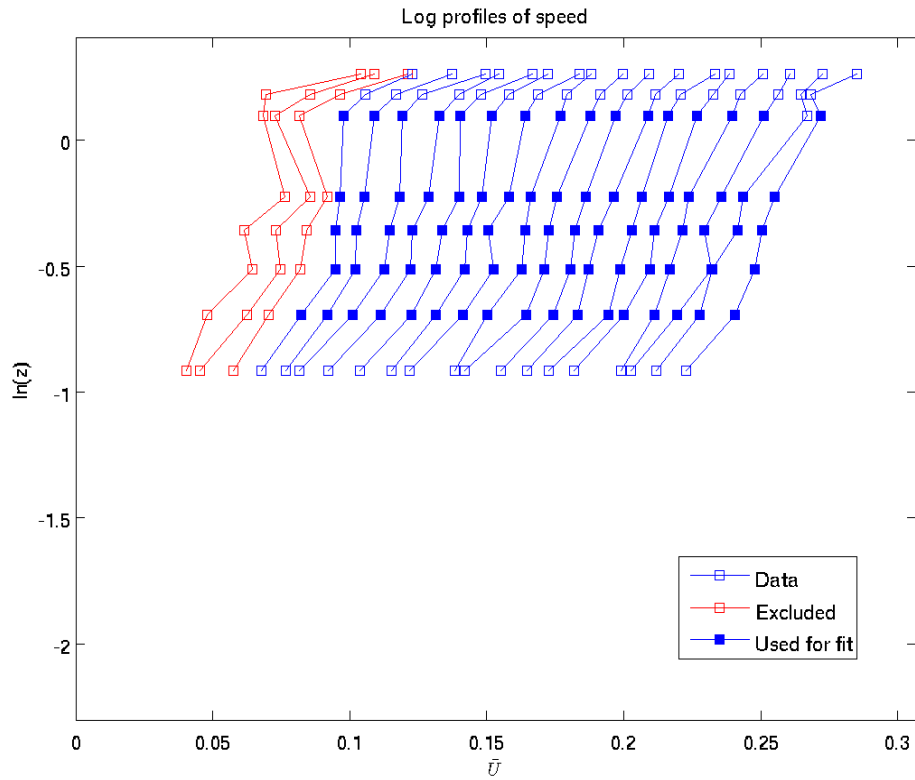
Figure 13 Profile plots of horizontal speed. Ensembles were averaged based on depth averaged velocity ranging from 6.5 to 26 cm/s in 1 cm/s increments.
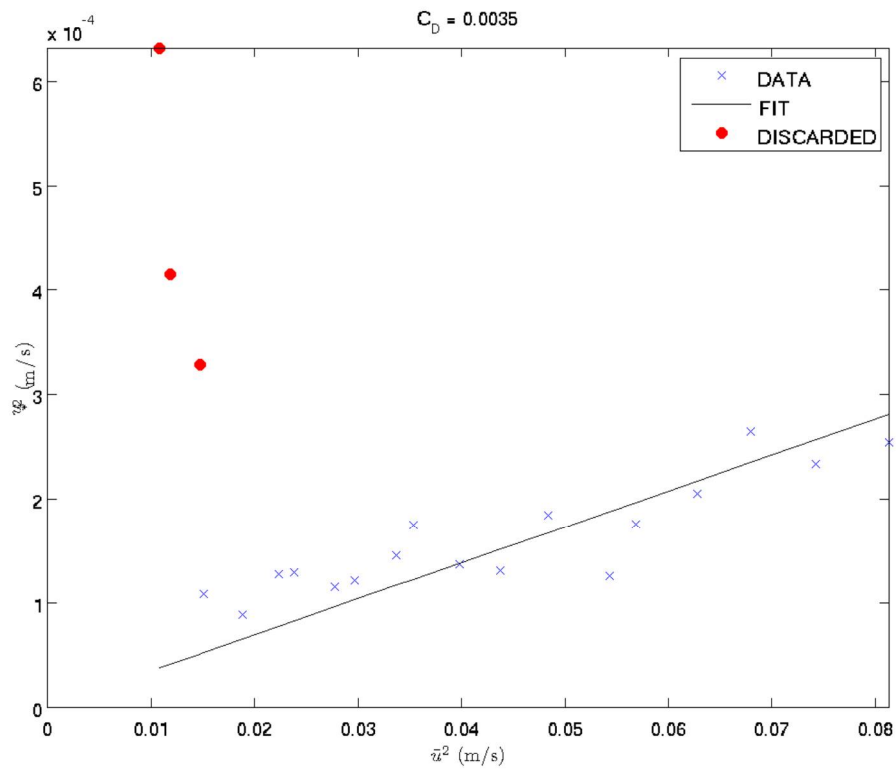

Figure 14 Best fit, forced through origin, of derived shear velocity U* to U, speed at 1.1 m above bottom to give bottom drag coefficient 3.5*10^-2
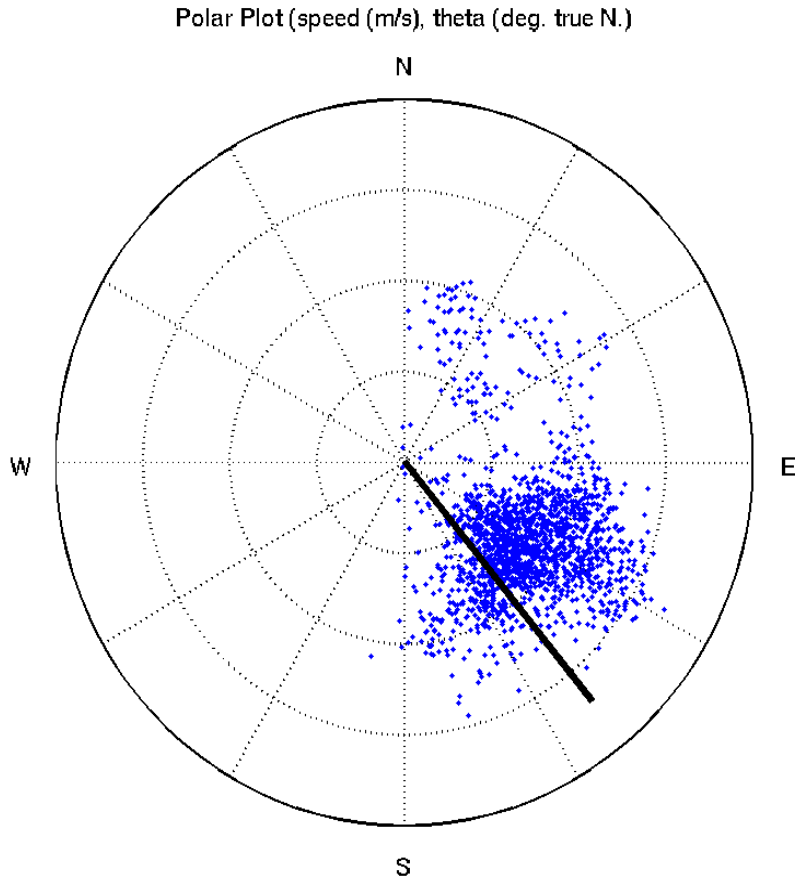
Figure 15 Polar plot with radius (in 0.1 m/s increment) representing horizontal speed from the bin closest to the AquaDopp, and theta representing direction the flow is going towards relative to true North. The solid black line is the heading of the AquaDopp relative to true north.